Detecting single photons is not always necessary to evidence interference of photon probability amplitudes

Eric Lantz [1,*] Fabrice Devaux,[1] and Serge Massar [2]

[1] *Département d'Optique, Institut FEMTO-ST, UMR 6174, CNRS, Université de Franche-Comté, 15 B rue des Montboucons, 25030 Besançon, France*

[2] *Laboratoire d'Information Quantique CP224, Université libre de Bruxelles, Avenue F. D. Roosevelt 50, 1050 Bruxelles, Belgium*

(Received 2 May 2024; revised 26 June 2024; accepted 11 July 2024; published 1 August 2024)

Subtracting accidental coincidences is a common practice in quantum optics experiments. For zero mean Gaussian states, such as a squeezed vacuum, we show that if one removes accidental coincidences, the measurement results are quantitatively the same for both photon coincidences at very low flux and intensity covariances. Consequently, pure quantum effects at the photon level, like interference of photon wave functions or photon bunching, are reproduced in the correlation of fluctuations of macroscopic beams issued from spontaneous down-conversion. This is true both in experiment if the detection resolution is smaller than the coherence cell (size of the mode) and in stochastic simulations based on sampling the Wigner function. We also discuss the limitations of this correspondence, such as Bell inequalities (for which one cannot subtract accidental coincidences), highly multimode situations such as quantum imaging, and higher-order correlations.

DOI: 10.1103/PhysRevA.110.023701

I. INTRODUCTION

Many iconic experiments in quantum optics, such as the Hong-Ou-Mandel (HOM) experiment [1], the demonstration of Einstein-Podolsky-Rosen (EPR) position-momentum correlations [2,3], and experimental tests of Bell inequalities [4], are based on correlations between detections of two photons. However, initial demonstrations of these experiments were done by subtracting accidental coincidences. Therefore, these initial experiments measured the covariance of the detection rates.

Later versions of these experiments were able to measure coincidences between single-photon detections without subtraction of accidental coincidences. For instance, this was achieved for the HOM experiment in [5,6], for the demonstration of EPR position-momentum correlations in [7], and for experimental tests of Bell inequalities in [8–11].

One of the aims of the present paper is to clarify the interpretation of experiments in which the covariance of detection rates is used. To illustrate how these notions appear in quantum optics, one can consider the correlations between two beams impinging on two photodiodes, D_1 and D_2 [as illustrated in Fig. 1(a)]. To this end one can use the mean of the product of the numbers of photons n_1 and n_2 detected, respectively, on D_1 and D_2, with a delay τ between the detections, $G_{12}^{(2)}(\tau) = \langle n_1 n_2 \rangle$, or its normalized version, $g_{12}^{(2)}(\tau) = G_{12}^{(2)}(\tau) \,/(\langle n_1 \rangle \langle n_2 \rangle)$. Alternatively, one can use the covariance $C_{12}(\tau) = \langle n_1 n_2 \rangle - \langle n_1 \rangle \langle n_2 \rangle$. The first quantity is often used to characterize a single-photon source. Indeed, if D_1 and D_2 are placed at the output of a balanced beam splitter, then $g_{12}^{(2)}(0)$ gives direct access to the purity of a single-photon source $1 - g^{(2)}(0)$, where $g^{(2)}$ is the autocorrelation function of the beam before the beam splitter [6]. [Indeed, it is easy to demonstrate that, in this detection scheme, $g^{(2)}(\tau) = g_{12}^{(2)}(\tau)$.] For a perfect single-photon source at zero delay, we have $g^{(2)}(0) = 0$, meaning that the detection of a photon on one photodiode prevents the simultaneous detection of a photon on the other photodiode, and consequently, the covariance is negative. On the other hand, the second quantity can be used to remove accidental coincidences when a measurement would otherwise be affected by excessive noise. For instance, in the original HOM experiment [1] performed with twin beams issued from spontaneous parametric down-conversion [SPDC; see Fig. 1(b)], the second quantity, i.e., the covariance, was measured, and "suppression of coincidences" meant zero covariance.

The aim of photodetection is to measure the number operator n. Due to technological limitations this measurement is always imperfect and falls into two broad categories. Single-photon detectors are generally of the on-off type: they are able to distinguish between the vacuum state $|0\rangle$ and states with one or more photons. When the average photon number $\langle n \rangle \ll 1$ is small, this is close to an ideal photon-number measurement. These detectors are affected by several imperfections, such as dark counts and limited efficiency. On the other hand, photodetectors, which are used at a higher average photon number, produce a current proportional to the number of photons, but with added noise that prevents the exact photon number from being resolved. Recently, photon-number-resolving detectors were developed with the capability of resolving up to a dozen photons (see, e.g., [12–14]). (For simplicity, we will not consider such detectors in the present paper.) One of the aims of the present work is to better understand the relation between experiments carried out in the low-flux regime, in which on-off single-photon

*Contact author: eric.lantz@univ-fcomte.fr

TABLE I. Status of subtraction of accidental coincidences or subtraction of the product of mean intensities.

	Subtraction of accidental coincidences	
Experiment	Very low flux	Higher flux
Characterization of twin photon sources	Optional	Necessary
HOM	Optional	Necessary
Bell	Forbidden	Forbidden
Purity of single-photon sources	Forbidden	Irrelevant

detectors are used, and in the high-power regime in which photodetectors with a continuous output are used. Better understanding this relation will provide answers to the following question: do we really need single-photon detectors to exhibit interferences of individual photons?

For definiteness, in the present work, we consider only the case used in many experiments today [15] in which photon pairs are produced via SPDC. First of all, we will show that when covariances are used, such experiments often have direct analogs in the high-power regime, where twin beams are very strongly correlated and in which the single-photon detectors would be replaced experimentally by photodetectors that measure light intensities. In this regime the intensity correlations exhibit the same behavior as the coincidence rate between single-photon detections. This is true for Bell experiments using SPDC, but we will see in Sec. III C that the classical reasoning leading to Bell inequalities involves products of intensities, not covariances. We summarize in Table I the status of subtraction of accidental coincidences in the different experiments considered in this paper.

In the present paper, we address some of the consequences of this equivalence between the low- and high-power regimes. First, the HOM experiment [1] can be considered the first experiment evidencing the existence of a photon without destroying it: two indistinguishable photons interfere in a balanced beam splitter and pursue together their path to one of the detectors, proving that photons do exist and are not a mere extrapolation of the quantification of the light-matter interaction [16]. It is worth noting and somewhat troubling that this experiment can be performed at sufficiently high power with photodetectors that measure light intensities, not individual photons. Note, however, that even at high power the twin beams are highly quantum: even if the intensity in each beam fluctuates, the two beams experience exactly the same fluctuations because of the photon pairs that constitute the beams. We aim to better understand the connection between the low- and high-power versions of this and other experiments.

A final important motivation for the present work concerns stochastic simulations of SPDC. This is a very useful tool for simulating quantum optics experiments (see, e.g., [17–21]). Indeed, stochastic sampling of the Wigner function is by far the fastest method to simulate highly multimode quantum optics experiments, providing considerable speedup compared to computing the biphoton wave function. However, as practitioners of this method know, using a (much) higher gain in simulations than in experiment leads to qualitatively similar results, but with a large saving in computational time. The present work helps us understand why one can use the high-gain regime in simulations: quantities like covariances will be similar in the low- and high-gain modes. We will illustrate this in Sec. IV B with an example based on a multimode HOM experiment.

Finally, we discuss limitations of the correspondence between the low- and high-gain regimes. We show that in experiments involving two photons, this correspondence is not perfect in the multimode case because the gains experienced by the different modes may not be all equal and may therefore not scale in the same way as one increases the pump power. This correspondence also breaks down in experiments involving more than two photons. And Bell experiments, of course, require single-photon detections. In Table I we list some iconic quantum optics experiments and indicate when the subtraction of accidental coincidences is allowed in both the low-flux and high-flux regimes. In the conclusion we discuss the implication of this correspondence for stochastic simulations of quantum optics experiments, as well as connections to hidden-variable models.

II. STOCHASTIC FIELD REPRESENTATION OF SYMMETRIZED CORRELATIONS

To address the above-mentioned correspondence between low- and high-power regimes, we use the Wigner representation as follows.

It was shown by Cahill and Glauber [22] [Eq. (4.23)] that the expectation value of a symmetrically ordered product of creation and annihilation operators $a^\dagger$ and a can always be expressed as an integral in the entire complex plane of the c-number α weighted by the Wigner function $W(\alpha)$:

$$\langle (a^\dagger)^n a^m \rangle_S = \frac{1}{\pi} \int_{\mathbb{C}} d^2\,\alpha (\alpha^*)^n \alpha^m W(\alpha). \tag{1}$$

Furthermore, [17,18,23] showed that the Wigner function for pump, signal, and idler fields in a $\xi^{(2)}$ medium obeys the classical equations of motion if the pump beam is undepleted, which is a good approximation in the cases studied here. Hence, if the initial Wigner function is Gaussian, then the Wigner function will stay Gaussian. We will use this below.

When the initial Wigner function of the signal and idler fields is positive (which is the case if they are in the vacuum), then these results provide an efficient way to compute numerically symmetrized products of creation and annihilation operators in highly multimode situations. To this end one randomly samples the initial signal and idler fields using the initial Wigner function as the probability distribution and then propagates—through the nonlinear crystal, beam splitters, focusing optics, etc.—these stochastic fields using the classical equations of motion. The average over the final distribution yields the desired expectation value. To obtain the expectation of normal ordered operators a correction is required, for instance, subtraction of the constant $1/2$ for the intensity and $1/4$ for the variance (when expressed in units of the photon number).

To illustrate the above we consider a SPDC experiment with two detectors at two distinct positions, D_1 and D_2. The symmetrized product of the corresponding field operators is given by the expectation of the stochastic classical fields,

$$\langle E_{D_1}^\dagger E_{D_1} E_{D_2}^\dagger E_{D_2}\rangle_S \equiv \frac{\langle (E_{D_1}^\dagger E_{D_1} + E_{D_1} E_{D_1}^\dagger)(E_{D_2}^\dagger E_{D_2} + E_{D_2} E_{D_2}^\dagger)\rangle}{4} = \langle E_{D_1} E_{D_1}^* E_{D_2} E_{D_2}^*\rangle, \quad (2)$$

where, on the left-hand side, we have the positive- and negative-frequency field operators and a quantum expectation value and, on the right, the expectation value of the classical stochastic fields. In the following we will generally work with the stochastic fields, which will be obvious from the notation, as they get complex conjugated $E_{D_1}^*$ rather than Hermitian conjugated $E_{D_1}^\dagger$.

Since the Wigner function is Gaussian, the fields at D_1 and D_2 obey the Gaussian moment theorem [24–26]:

$$\langle E_{D_1} E_{D_1}^* E_{D_2} E_{D_2}^*\rangle = \langle E_{D_1} E_{D_1}^*\rangle\langle E_{D_2} E_{D_2}^*\rangle + \langle E_{D_1} E_{D_2}^*\rangle\langle E_{D_2} E_{D_1}^*\rangle + \langle E_{D_1} E_{D_2}\rangle\langle E_{D_1}^* E_{D_2}^*\rangle . \quad (3)$$

Equation (3) can be rewritten in terms of detected intensities $I_{D_1} = E_{D_1} E_{D_1}^*$ and $I_{D_2} = E_{D_2} E_{D_2}^*$ as

$$\langle I_{D_1} I_{D_2}\rangle = \langle I_{D_1}\rangle\langle I_{D_2}\rangle + |\langle E_{D_1} E_{D_2}^*\rangle|^2 + |\langle E_{D_1} E_{D_2}\rangle|^2 .$$

Reorganizing terms, we obtain an expression for the covariance:

$$\mathrm{cov}(I_{D_1}, I_{D_2}) = \langle I_{D_1} I_{D_2}\rangle - \langle I_{D_1}\rangle\langle I_{D_2}\rangle = |\langle E_{D_1} E_{D_2}^*\rangle|^2 + |\langle E_{D_1} E_{D_2}\rangle|^2 . \quad (4)$$

Because of the subtraction of the product of the mean intensities (unlike in the G_2 coefficient), the covariance between the detected intensities can therefore be deduced from two mean products of two stochastic fields. In practice, only one mean product remains: one of the two means vanishes because only phase differences make sense. This mean product of stochastic fields has a form similar to the product of creation operators in the biphoton wave function. Hence, the behavior of the covariance of signal-idler intensities is the same as the correlation of the signal and idler photons in a pair. This is true in a vast number of quantum optics experiments using SPDC, both at very low fluxes, where photon coincidences are detected, and for intense twin beams, where one measures intensities without photon resolution. It can be noted that the formalism of the biphoton concerns a single pair and, consequently, is valid in a regime of very low flux where the probability of accidental coincidences is weak and can be neglected. In such a regime, results are similar with and without subtraction of coincidences: as quoted in Table I, this subtraction is optional. On the other hand, at high flux this subtraction, or the subtraction of the product of mean intensities, is necessary to keep only the same product of two fields as at low flux.

We note also that in the high-intensity case one needs to use photodetectors with resolution much smaller than the coherence cell (size of the mode) in the time domain as well as in the space domain. Otherwise, the fluctuations will be averaged out. On the other hand, in the low-intensity regime, when single-photon detectors are used, the time and space windows can be much larger than the coherence length, provided the probability of a single photon being detected in each window is much smaller than 1. In this regime the subtraction of the accidental coincidences [the second term in Eq. (4)] is not compulsory. It improves the results, but the accidental coincidence term can be much smaller than the true coincidence term. The accidental coincidences in this regime could come from pairs in different modes or from dark counts.

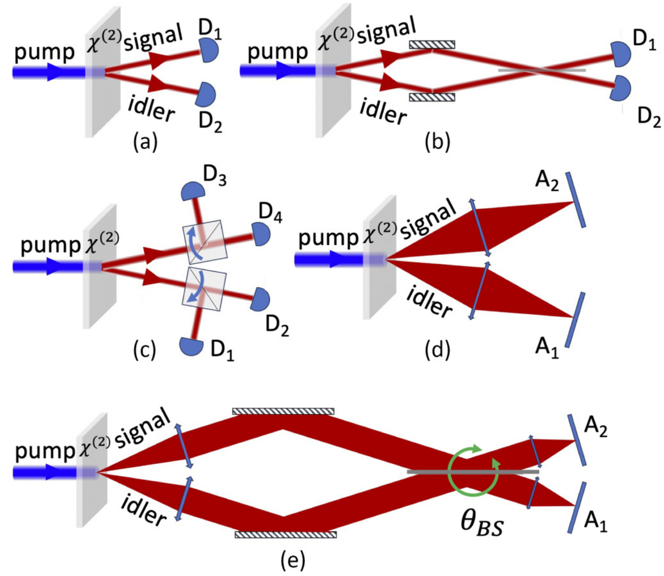

FIG. 1. Experimental setups considered in this work: (a) nondegenerate parametric down-conversion (PDC), (b) Hong-Ou-Mandel (HOM) experiment, (c) Bell experiment, (d) multimode nondegenerate PDC, and (e) HOM with multimode nondegenerate PDC. In (d) and (e), A_1 and A_2 are the imaging planes of cameras (possibly with single-photon resolution). The pump beam is in blue; signal and idler photons produced by PDC are in red. In (e), $\theta_{\rm BS}$ represents an angular shift of the beam splitter, used in the abscissa in Fig. 2.

III. EXAMPLES

A. Nondegenerate SPDC

We now give some examples of the use of (4) to establish well-known results usually deduced from the biphoton wave function. These examples are illustrated in Fig. 1.

We first consider the very simple case of nondegenerate SPDC and direct detection, at the output of the crystal, of the intensities I_s and I_i of the signal and idler beams, respectively. At perfect phase matching, the classical equations of parametric amplification give, for a single pair of signal and idler fields E_s and E_i after amplification in a crystal of length L,

$$E_s(L) = CE_s(0) - iSE_i^*(0),$$
$$E_i(L) = CE_i(0) - iSE_s^*(0), \quad (5)$$

where $C = \cosh(gL)$ and $S = \sinh(gL)$, with g being the gain per length unit, proportional to the pump amplitude. The phases are defined with respect to the pump.

Using the fact that $E_s(0)$ and $E_i(0)$ are independent vacuum fields, each with a mean intensity of 1/2 in units of photons per mode [22,27], we obtain from (4)

$$\langle E_s(L)E_s(L)\rangle = \langle E_i(L)E_i(L)\rangle = \langle E_s(L)E_i^*(L)\rangle = 0$$

and

$$\begin{aligned}\mathrm{cov}(I_s(L), I_i(L)) &= |\langle E_s(L)E_i(L)\rangle|^2\\ &= C^2S^2\langle E_s(0)E_s^*(0) + E_i(0)E_i^*(0)\rangle^2\\ &= C^2S^2 \,. \end{aligned} \tag{6}$$

We can also calculate the mean intensity and the variance:

$$\begin{aligned}\langle I_s(L)\rangle &= \langle E_s(L)E_s^*(L)\rangle - 1/2\\ &= C^2\langle E_s(0)E_s^*(0)\rangle + S^2\langle E_i(0)E_i^*(0)\rangle - 1/2\\ &= S^2,\end{aligned}$$

$$\begin{aligned}\mathrm{var}[I_s(L)] &= |\langle E_s(L)E_s^*(L)\rangle|^2 - 1/4\\ &= \langle C^2E_s(0)E_s^*(0) + S^2E_i(0)E_i^*(0)\rangle^2 - 1/4\\ &= C^2S^2.\end{aligned} \tag{7}$$

The subtraction of 1/2 for the intensity and 1/4 for the variance is necessary to pass from the symmetrized order to the normal order [22,27], while this correction is zero for covariances.

We note that the variance of one of the twin beams is equal to the covariance between the beams. Thus, even at high flux, the beams are perfectly correlated.

The quantum efficiency η of the detectors is easily taken into account by adding fictitious beam-splitters that mix the actual fields with vacuum fields:

$$\begin{aligned}E_{D_1} &= \sqrt{\eta}E_s + \sqrt{1-\eta}E_{v_1},\\ E_{D_2} &= \sqrt{\eta}E_i + \sqrt{1-\eta}E_{v_2},\end{aligned} \tag{8}$$

where E_{v_1} and E_{v_2} are two independent vacuum fields. As detailed in Appendix A, a straightforward calculation using (8), (4), and (5) leads to

$$\begin{aligned}\mathrm{var}(I_{D_1}) = \mathrm{var}(I_{D_2}) &= \eta^2S^4 + \eta S^2,\\ \mathrm{cov}(I_{D_1}, I_{D_2}) &= \eta^2S^4 + \eta^2S^2 \,.\end{aligned} \tag{9}$$

The fluctuations of the classical intensity (first terms) remain perfectly correlated. This result should be contrasted with the shot noise (second terms): random deletion of photons leads to detection of photons without a twin.

B. Hong-Ou-Mandel experiment

We now move to the HOM experiment [1] [see Fig 1(b)]. As in the original experiment, we assume that the signal and idler photons are made indistinguishable by rotation of polarization and arrive at the two input ports, s and i, of a balanced and lossless beam splitter, with output ports labeled 1 and 2. Conservation of energy imposes

$$\begin{aligned}&|t_{s_1}|^2 + |r_{s_2}|^2 = |t_{i_2}|^2 + |r_{i_1}|^2 = 1,\\ &t_{s_1}r_{s_2}^* + r_{i_1}t_{i_2}^* = 0,\end{aligned} \tag{10}$$

where t_{k_l} (r_{k_l}), with $k = s, i$ and $l = 1, 2$, are the transmission (reflection) coefficients from k to l, in amplitude. We obtain

$$\begin{aligned}E_1 &= t_{s_1}E_s + r_{i_1}E_i,\\ E_2 &= r_{s_2}E_s + t_{i_2}E_i,\end{aligned}$$

$$\begin{aligned}\mathrm{cov}(I_1, I_2) &= |\langle E_1E_2^*\rangle|^2 + |\langle E_1E_2\rangle|^2\\ &= |(t_{s_1}t_{i_2} + r_{i_1}r_{s_2})\langle E_sE_i\rangle|^2.\end{aligned} \tag{11}$$

To establish (11), we used (10), $\langle E_sE_s^*\rangle = \langle E_iE_i^*\rangle$ and $\langle E_sE_s\rangle = \langle E_iE_i\rangle = \langle E_sE_i^*\rangle = 0$. If the beam splitter is balanced, $t_{s_1}t_{i_2} + r_{i_1}r_{s_2} = 0$, and we obtain, as expected, $\mathrm{cov}(I_1, I_2) = 0$.

We emphasize that this result holds both in the low-gain (single-photon) regime and in the high-gain (photodetector) regime.

C. Bell experiment

Our next example concerns the Bell state $\frac{1}{\sqrt{2}}(|H_1V_2\rangle + |V_1H_2\rangle)$, where 1 and 2 denote two distinct locations where the two photons of a pair are respectively detected and H and V stand for horizontal and vertical polarizations [see Fig. 1(c)]. SPDC is the most often used way to produce such entangled pairs; for instance, Kwiat *et al.* [28] showed how to obtain such a state at the double intersection of the two cones of type-II SPDC.

If the signal and idler are horizontally and vertically polarized along x and y, respectively, then the fields E_{1+} and E_{2+} at locations 1 and 2 after passing through polarizing beam splitters oriented along θ_1 and θ_2 are written as

$$\begin{aligned}E_{1+} &= E_{1x}\cos(\theta_1) + E_{1y}\sin(\theta_1),\\ E_{2+} &= E_{2x}\cos(\theta_2) + E_{2y}\sin(\theta_2).\end{aligned} \tag{12}$$

Using (6), this leads to a covariance between the respective intensities I_{1+} and I_{2+}:

$$\begin{aligned}\mathrm{cov}(I_{1+}, I_{2+}) &= |E_{1+}E_{2+}|^2\\ &= |E_{1x}E_{2y}\cos(\theta_1)\sin(\theta_2)\\ &\quad + E_{1y}E_{2x}\sin(\theta_1)\cos(\theta_2)|^2\\ &= C^2S^2\sin^2(\theta_1+\theta_2).\end{aligned} \tag{13}$$

By dividing by the variance given in (7), we obtain the correlation coefficient,

$$\rho = \frac{\mathrm{cov}(I_{1+}, I_{2+})}{\sqrt{\mathrm{var}(I_{1+})\mathrm{var}(I_{2+})}} = \sin^2(\theta_1+\theta_2), \tag{14}$$

which has exactly the same form as the probability of detecting two photons in this configuration. Thus, by replacing the product of the intensities by their correlation coefficients in the Clauser-Horne-Simony-Holt (CHSH) inequalities [29], we can retrieve, whatever the field intensity, the same value of the Bell parameter B as for a biphoton state, with a well-known maximum of $2\sqrt{2}$.

However, the above does not provide a violation of the CHSH inequality because the positivity of intensities is one of the ingredients that is used to derive the CHSH inequality. For instance, if we follow the reasoning presented in [30,31], there is a step which uses the inequality:

$$\left|\frac{I_+ - I_-}{I_+ + I_-}\right| < 1, \tag{15}$$

where I_+ and I_- are the two output intensities of one of the polarizing beam splitters. Using covariances is equivalent to replacing I_+ (I_-) by $I_+ - \langle I_+\rangle$ ($I_- - \langle I_-\rangle$), but then these quantities are not always positive and do not fulfill condition (15).

It is, nevertheless, possible to use our approach to calculate the maximum gain G that allows the Bell inequalities to be violated (giving only a threshold separating the regime of nonlocal pairs and the regime of correlated intensities, not proof that this is the actual threshold). It is, indeed, easy to show from (12) and (5) that, whatever the angles,

$$G = \langle I_{1+}\rangle = \langle I_{1-}\rangle = \langle I_{2+}\rangle = \langle I_{2-}\rangle = S^2, \tag{16}$$

leading, using (13), to

$$\begin{aligned}\langle I_{1+}I_{2+}\rangle = \langle I_{1-}I_{2-}\rangle = C^2S^2\sin^2(\theta_1+\theta_2)+S^4,\\ \langle I_{1+}I_{2-}\rangle = \langle I_{1-}I_{2+}\rangle = C^2S^2\cos^2(\theta_1+\theta_2)+S^4.\end{aligned} \tag{17}$$

Upon inserting this into the Bell expression B, one finds, after some manipulations, that

$$B(G) = \frac{1+G}{1+3G}B(0), \tag{18}$$

where $B(0)$ is the Bell parameter at vanishing gain and $B(G)$ is the Bell parameter at gain G. To violate the CHSH inequality we need $B(G) > 2$ while $B(0) = 2\sqrt{2}$, leading to the threshold for violation of the CHSH inequality $\frac{1+G}{1+3G} < \frac{1}{\sqrt{2}}$. This was stated in a different, but equivalent, form in [31], using the Heisenberg point of view and in this form in [27] and then in [32]. The approach developed here appears particularly simple. The details of the calculation are given in Appendix B.

D. Multimode case

We now discuss how to take into account the multimode character of the SPDC. We consider, for definiteness, spatial degrees of freedom, as illustrated in Fig. 1(d), although the same reasoning would apply for temporal degrees of freedom. We consider two detector planes, and we label the pixels of the detector array on the signal side with a subscript l and on the idler side with a subscript m. For a given crystal length L, the mean product of signal-idler fields used in the calculation of the covariance in (6) can be expressed, using the singular-value decomposition [33], as

$$\langle Es_l Ei_m\rangle = \sum_k U_{lk}\lambda_k V_{mk}, \tag{19}$$

with U and V being unitary matrices and $0 \leqslant \lambda_k$ being the singular values. A gain g_k can be defined for each mode k as

$$\lambda_k = \cosh(g_k)\sinh(g_k) = C_kS_k. \tag{20}$$

The fields in each pair of Schmidt modes can be written as in (5):

$$\begin{aligned}Es_k(L) = C_kEs_k(0) - iS_kEi_k^*(0),\\ Ei_k(L) = C_kEi_k(0) - iS_kEs_k^*(0).\end{aligned} \tag{21}$$

The actual fields remain Gaussian since they result from the superposition of the Gaussian Schmidt fields:

$$\begin{aligned}Es_l = \sum_k U_{lk}Es_k,\\ Ei_m = \sum_k V_{mk}Ei_k.\end{aligned} \tag{22}$$

Because U and V are unitary, Eqs. (6), (21), and (22) lead to (19). More generally, the unitarity of these matrices means that all the above monomode relations have a multimode equivalent, with a gain which is mode dependent. For example, the intensity on a pixel on the signal side can be written in an analogous way to Eq. (7):

$$\begin{aligned}Is_l &= \langle Es_lEs_l^*\rangle - 1/2\\ &= \Big\{\sum_k |U_{lk}|^2[C_k^2\langle Es_k(0)Es_k^*(0)\rangle\\ &\quad + S_k^2\langle Ei_k(0)Ei_k^*(0)\rangle]\Big\} - 1/2\\ &= \sum_k |U_{lk}|^2S_k^2.\end{aligned} \tag{23}$$

Analyzing the spatiotemporal variation of correlations in detail is beyond the scope of this paper. The analysis in the temporal domain was already detailed in the original HOM paper [1]. For a numerical and experimental analysis of spatiotemporal effects in the HOM experiment, see [20,21]. Here, we would like to stress that the simple fact that the fields are Gaussian means that Eq. (4) remains valid: for SPDC, the analysis of intensity covariances can be performed at high intensities and gives the same results as the analysis of photon coincidences at low flux.

The main difference from the single-mode case is that, because the different modes have different gains, changing the power of the pump laser in a multimode SPDC experiment will not simply multiply all intensities and correlation coefficients by a particular factor. Thus, a high gain allows the amplification of modes that are not perfectly phase matched. Hence, in a HOM experiment [see Fig. 1(e) for the spatial multimode case], a higher gain leads to a wider bandwidth in the spatial or temporal frequency domain. This is illustrated in Fig. 2 by the simulation of a spatial multimode HOM experiment with varying pump power. However, the small dependence of the dip in Fig. 2 as a function of pump power means that one can use the simulations at high power, which are much faster, to describe with high precision the experiment in the low-power, photon-counting regime.

E. Multiparticle correlations

The above considerations were made for correlations between two intensities. How does this generalize to correlations between more than two intensities? For definiteness, we consider the fourfold correlation between two signal intensities, detected in two close locations, s_1 and s_2, separated by less than the size of the coherence cell, and two idler intensities in two close locations, i_1 and i_2 [34].

The fourfold covariance

$$C_o = (I_{s_1} - \langle I_{s_1}\rangle)(I_{s_2} - \langle I_{s_2}\rangle)(I_{i_1} - \langle I_{i_1}\rangle)(I_{i_2} - \langle I_{i_2}\rangle) \tag{24}$$

has nine terms. To see this, we reason as follows:

(1) Using the Gaussian moment theorem, we find that the fields E_{s_1}, E_{s_2}, $E_{i_1}^*$, and $E_{i_2}^*$ give nonzero terms only when associated with the fields $E_{s_1}^*$, $E_{s_2}^*$, E_{i_1}, and E_{i_2} [see (6)], resulting in $4! = 24$ terms in $\langle I_{s_1}I_{s_2}I_{i_1}I_{i_2}\rangle$.

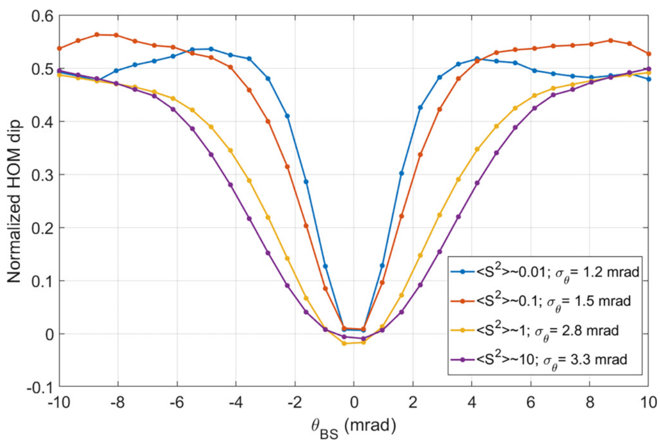

FIG. 2. Influence of the gain $\langle S^2\rangle$ in a multimode HOM experiment realized using the setup illustrated in Fig. 1(e), obtained using stochastic simulations. The gains in the different curves correspond to average numbers of photons per pixel of 0.01, 0.1, 1, and 10. On the abscissa, $\theta_{\rm BS}$ is the rotation angle of the beam splitter used to control momentum indistinguishability between the signal and idler beams. The horizontal angular shift of the reflected beams is 2 times $\theta_{\rm BS}$. The results of numerical simulations using the stochastic model are averaged over 100 iterations. The crystal length is $L = 0.8$ mm. On the ordinate, the normalized amplitude of the HOM dip is obtained by dividing the correlation between the two output far-field images by the correlation between the two input far-field images. The correlation is obtained by dividing the covariance by the square root of the product of the variances [see Eq. (14)]. Note that as the gain changes by 4 orders of magnitude, the width σ_θ changes by less than a factor of 3. (The width σ_θ given in the legend is obtained from Gaussian fits to the numerical data). Note that the curves at low gain are noisier (especially in the wings of the curves), in contrast to the curves at high gain.

(2) Hence, C_o has 24 terms from $\langle I_{s1}I_{s_2}I_{i1}I_{i2}\rangle$ minus $4\times 6 = 24$ terms with a mean intensity times a threefold product like $\langle I_{s_1}\rangle\langle I_{s_2}I_{i_1}I_{i_2}\rangle$ plus $6\times 2 = 12$ terms with a product of two mean intensities minus 4 terms with three mean intensities plus 1 term product of the four mean intensities. The 15 removed terms include at least a mean intensity, and this is precisely the number of terms in $\langle I_{s_1}I_{s_2}I_{i_1}I_{i_2}\rangle$, which include such a mean.

Hence, C_o includes only the nine terms without a mean intensity:

$$C_o = \langle E_{s_1}E^*_{s_2}\rangle\langle E_{s_2}E^*_{s_1}\rangle\langle E^*_{i_1}E_{i_2}\rangle\langle E^*_{i_2}E_{i_1}\rangle \tag{25}$$
$$+\langle E_{s_1}E^*_{s_2}\rangle\langle E_{s_2}E_{i_1}\rangle\langle E^*_{i_1}E_{i_2}\rangle\langle E^*_{i_2}E^*_{s_1}\rangle \tag{26}$$
$$+\langle E_{s_1}E^*_{s_2}\rangle\langle E_{s_2}E_{i_2}\rangle\langle E^*_{i_1}E^*_{s_1}\rangle\langle E^*_{i2}E_{i_1}\rangle \tag{27}$$
$$+\langle E_{s_1}E_{i_1}\rangle\langle E_{s_2}E^*_{s_1}\rangle\langle E^*_{i_1}E_{i_2}\rangle\langle E^*_{i_2}E^*_{s_2}\rangle \tag{28}$$
$$+\langle E_{s_1}E_{i_1}\rangle\langle E_{s_2}E_{i_2}\rangle\langle E^*_{i_1}E^*_{s_1}\rangle\langle E^*_{i_2}E^*_{s_2}\rangle \tag{29}$$
$$+\langle E_{s_1}E_{i_1}\rangle\langle E_{s_2}E_{i_2}\rangle\langle E^*_{i_1}E^*_{s_2}\rangle\langle E^*_{i_2}E^*_{s_1}\rangle \tag{30}$$
$$+\langle E_{s_1}E_{i_2}\rangle\langle E_{s_2}E^*_{s_1}\rangle\langle E^*_{i_1}E_{i_2}\rangle\langle E^*_{i_2}E^*_{s_2}\rangle \tag{31}$$
$$+\langle E_{s_1}E_{i_2}\rangle\langle E_{s_2}E_{i_1}\rangle\langle E^*_{i_1}E^*_{s_1}\rangle\langle E^*_{i_2}E^*_{s_2}\rangle \tag{32}$$
$$+\langle E_{s_1}E_{i_2}\rangle\langle E_{s_2}E_{i_1}\rangle\langle E^*_{i_1}E^*_{s_2}\rangle\langle E^*_{i_2}E^*_{s_1}\rangle. \tag{33}$$

These terms scale differently as a function of the gain.

Term (25) is a term of incoherent bunching, proportional to S^8.

The terms

$$(29)+(30)+(32)+(33) = |E_{s_1}E_{i_1}E_{s_2}E_{i_2} + E_{s_1}E_{i_2}E_{s_2}E_{i_1}|^2, \tag{34}$$

proportional to C^4S^4, are the only ones that remain at low gain. They can result in interferences in the four-photon coincidences [34].

The four remaining terms, proportional to C^2S^6, have a less clear interpretation. They can be written as

$$(26)+(27)+(28)+(31) = \{\langle E_{s_1}E^*_{s_2}\rangle(\langle E_{s_2}E_{i_1}\rangle\langle E^*_{i_1}E_{i_2}\rangle\langle E^*_{i_2}E^*_{s_1}\rangle + \langle E_{s_2}E_{i_2}\rangle\langle E^*_{i_1}E^*_{s_1}\rangle\langle E^*_{i_2}E_{i_1}\rangle)\} + \text{c.c.} \tag{35}$$

These relations can be extended to the multimode case, most easily using the singular-value decomposition (19).

IV. DISCUSSION

A. Correspondence between low- and high-power experiments

The first message conveyed here is that purely quantum effects, intimately linked to the particle character of photons, have an exact counterpart in the fluctuations of macroscopic twin beams. These macroscopic twin beams are not classical beams: they are formed by pairs and possess quantum properties [35]. For example, if the photon number of each beam strongly fluctuates with a thermal statistics, the fluctuations of both beams are strictly the same, and the variance of the difference of photon numbers is exactly zero in an ideal experiment [36]. A practical illustration is the use in quantum imaging experiments of a variance of the difference in photon numbers smaller than the Poisson noise to prove the particle character of twin images [2,37–39]. Furthermore, with twin macroscopic beams, the visibility of interference in a HOM experiment is not limited to 0.5, as is the case for classical beams [40,41], but can go down to zero. Thus, the HOM interference for a photon pair can be generalized to the interference of many photon pairs in a single mode, with covariance as the quantity that is used in both situations. Subtracting accidental coincidences is a useful procedure not only to eliminate the effect of independent pairs coming from other modes (or electronic noise) but also to take into account correlated pairs in a mode, obeying a Bose-Einstein (thermal) statistics. If the use of the subtraction of accidental coincidences to remove noise coming from other modes is quite obvious, the use of covariance even inside a single mode is much less intuitive but is correct for Gaussian statistics. Bell inequalities are an exception: they use products of intensities, not their covariance. Indeed, the violation of Bell inequalities describes the nonlocal character of the correlation of two photons forming a unique pair.

B. Stochastic simulations

The second message concerns stochastic simulations, which are a very useful tool for simulating quantum optics experiments (see, e.g., [17–19]). Indeed, stochastic sampling of the Wigner function is by far the fastest method to simulate highly multimode quantum optics experiments, such as quantum imaging involving an image of N by N pixels. Indeed, the computation time will be proportional to N^2. In comparison, the computation time of the biphoton wave function is at least proportional to N^6 [42]. For recent illustrations of the application of this method, we refer to highly spatially multimode HOM experiments presented in [20,21],

As practitioners of this method know, using a (much) higher gain in simulations than in experiment leads to qualitatively similar results, but with a large saving in computational time. The reasons for the qualitative similarity of the results is explained by the present analysis: quantities like covariances will be similar in the low- and high-gain modes. The (small) differences are due, for instance, to phase-matching conditions: a high gain allows the amplification of some modes that are not perfectly phase matched [43]. As an illustration, in a HOM experiment, a higher gain leads to a slightly wider bandwidth in the spatial or temporal frequency domain. This is illustrated in Fig. 2 for the spatial HOM experiment described in Fig. 1(e). We see that, whatever the gain, the covariance falls close to zero in the center of the dip, validating the use in numerics of a higher gain than in the experiment.

The advantage of using a high gain in simulation is drastic: stochastic simulations with a low gain imply a huge number of repetitions of the simulation to obtain an acceptable signal-to-noise ratio (SNR). This is due to the fact that the signal has the level of the actual intensity without the input vacuum noise, while the noise includes this vacuum noise [44]. Thus, for a small gain the SNR (defined as the ratio between the mean intensity and its standard deviation) will be equal to the average number of photons per mode (which in experimental situations will be 0.1 or less). On the other hand, with a gain of many photons per mode, the influence of the input vacuum noise on the SNR becomes negligible. Thus, with a high gain and for one repetition, the SNR is equal to 1 because of the Bose-Einstein statistics of the intensity. Hence, for R repetitions, the SNR is equal to $\sqrt{R}$. The total computational cost will thus be $R \times N^2$.

On the experimental side, using high gain to demonstrate quantum effects at the photon level is possible in principle but less evident than in simulations. The principal reason is that the time resolution of the detectors is often much greater than the duration of a SPDC mode, given by the inverse of the spectral bandwidth of phase matching or of the added spectral filter, if any. In the 1987 HOM experiment [1], the time window for coincidences of twin photons was 7 ns for a coherence time of about 100 fs. With such timescales, the fluctuations of more than 10^4 independent modes would be averaged if a high-intensity beam was used. An obvious solution to work in the quasimonomode regime is to use short pulses and narrow spectral filters with a time separation of the pulses smaller than the time window of the detectors. This was done in [37,45–47]. Eisenberg *et al.* [45] analyzed two-photon coincidences with a small quantum efficiency and up to 50 photons per mode. However, their use of on-off detectors led to a strong distortion of the statistics. For example, at high fluxes, the probability of coincidences tends to 1, and the covariance tends to zero. In [46], photon-number-resolving detectors were employed. For images, Jedrkiewicz *et al.* demonstrated [37] the sub-shot-noise character of the difference between signal-idler images issued from type-II SPDC with 100 photons per mode. In [47], high-intensity images produced by type-I SPDC were obtained and used to demonstrate the Bose-Einstein character of the statistics, and an image was reported in which the twin character of the signal-idler fluctuations was clearly visible but not quantitatively analyzed.

C. A hidden-variable model

Stochastic simulations use the propagation of classical fields to reproduce the predictions of quantum experiments. We discuss here their connection with hidden-variable models of quantum mechanics. Such hidden-variable models are interesting because they can, in some cases, provide an intuitive, classical picture of the underlying quantum phenomena. Ideally,

such a hidden-variable model should have the following characteristics:

(1) The hidden-variable model reproduces the outcomes of one or several observables. That is, individual realizations of the hidden-variable model predict individual outcomes of the observable, with the correct probability distribution being reproduced when averaged over the hidden variables.

(2) The hidden-variable model is local; that is, when describing multiparticle systems, one can assign hidden variables to each particle, and the evolution of these hidden variables depends only on the local environment of each particle.

Bell's theorem [48] proves that one cannot satisfy both requirements. Bohm's model [49] shows that the first requirement can be met for position measurements of single particles. But Bohm's model, or extensions thereof, cannot be extended to a local model of two or more entangled particles (since, otherwise, a contradiction with Bell's theorem would occur).

The stochastic simulations of quantum optics experiments satisfy the second requirement since the fields are propagated using the classical equations of motion and hence are local but do not satisfy the first requirement. To see this explicitly, consider the symmetrized number operator $(a^\dagger a + aa^\dagger)/2$. This operator has half-integer eigenvalues $1/2, 3/2, \ldots$. The stochastic model will, at each repetition, yield a positive real value for the symmetrized number operator. The average will yield the correct expectation value [see Eq. (1)]. But the individual runs cannot be used so simulate individual outcomes of the measurement (otherwise, a contradiction with Bell's theorem would occur). This can also be seen from the fact that individual runs can yield values less than $1/2$, corresponding to a negative photon number, which would be unphysical.

A fundamental difference remains, however, between the low- and high-flux regimes. At high flux, a detection proportional to intensity is described by projection onto a positive Wigner function, meaning that one repetition of the experiment or of the corresponding stochastic simulation can be drawn from the same probability distribution [50,51]. On the other hand, the on-off detectors used at low flux correspond to a projection on a one-photon state with a partially negative Wigner function. In this regime, as mentioned above, there is no correspondence between the experimental and simulated samples. For example, a sample in a simulation can correspond to a negative intensity after the subtraction required to obtain the normal ordered operator. Only the covariance, i.e., the mean over a large number of repetitions, is identical in simulations and experiments.

As a final remark, an alternative exists to simulate measurement outcomes at very low flux: the photon pairs can be considered independent, and the probability distribution can be directly inferred from the square biphoton amplitude. The simulation of experimental samples, i.e., sampling from the classical probability distribution, appears particularly difficult in the intermediate situation, with a gain neither much lower nor much higher than 1. Indeed, this is a situation similar to boson sampling, where it is expected that such sampling is computationally hard. For a study of quantum imaging experiments in this regime, see [34].

D. Summary

In the present work we have not presented any new quantum optics results. Rather, we have clarified the connection between low-flux and high-flux quantum optics experiments through the lens of stochastic field simulations. For Gaussian states like SPDC, we have shown that the covariance describes coincidences of photons at very low flux as well as correlations of intensity fluctuations at high flux. We have retrieved for covariances some well-known results for coincidences, like the disappearance of coincidences in the HOM experiment. The computations are analogous to those based on the biphoton wave functions but are valid for any number of photon pairs in a mode. We have treated only some simple cases, but an extension to more realistic or more complex situations can readily be carried out. The same results can, of course, also be obtained by using the Heisenberg representation, but the connection to the biphoton state is less evident. Our work also shows why high-gain stochastic simulations of an experimental setup (which are computationally efficient) will generally yield results close to those obtained in the experimental, low-gain regime. Finally a conceptual link to hidden-variable models was discussed.

APPENDIX A: DERIVATION OF EQ. (9)

We detail here the computation leading to expressions (9) for the variance and covariance for a nonunity quantum efficiency η. As stated in the main text, the addition of a fictitious beam splitter before the detectors leads to Eq. (8):

$$\begin{aligned} E_{D_1} &= \sqrt{\eta}E_s(L) + \sqrt{1-\eta}E_{v_1}, \\ E_{D_2} &= \sqrt{\eta}E_i(L) + \sqrt{1-\eta}E_{v_2}, \end{aligned}$$

leading to a mean intensity on the photodiode D_1:

$$\begin{aligned} \langle I_{D_1}\rangle &= \langle E_{D_1}E^*_{D_1}\rangle - 1/2 \\ &= \langle E_s(L)E^*_s(L)\rangle + (1-\eta)\langle E_{v_1}E^*_{v_1}\rangle - 1/2 \\ &= \eta(C^2+S^2)/2 + (1-\eta)/2 - 1/2 \\ &= \eta S^2. \end{aligned} \tag{A1}$$

As expected, the intensity is simply multiplied by the quantum efficiency.

The variance is computed in the same way:

$$\begin{aligned} \mathrm{var}(I_{D_1}) &= \langle (E_{D_1}E^*_{D_1})^2\rangle - 1/4 \\ &= \eta^2[(C^2+S^2)/2]^2 + \eta(1-\eta)(C^2+S^2)/2 \\ &\quad + 1/4(1-\eta)^2 - 1/4 \\ &= \eta^2 S^4 + \eta S^2. \end{aligned} \tag{A2}$$

The computation of the covariance between the intensities in D_1 and D_2 is simpler since the vacuums v_1 and v_2 are not correlated:

$$\begin{aligned} \mathrm{cov}(I_{D_1}, I_{D_2}) &= |\langle\langle E_{D_1}E_{D_2}\rangle\rangle|^2 \\ &= \eta^2|\langle E_s(L)E_i(L)\rangle|^2 \\ &= \eta^2C^2S^2 = \eta^2S^4 + \eta^2S^2. \end{aligned} \tag{A3}$$

APPENDIX B: DERIVATION OF EQ. (18)

The coefficients used in the CHSH inequalities have the form

$$\begin{aligned} E(\theta_1,\theta_2) &= \frac{\langle I_{1+}I_{2+} + I_{1-}I_{2-} - I_{1+}I_{2-} - I_{1-}I_{2+}\rangle}{\langle I_{1+}I_{2+} + I_{1-}I_{2-} + I_{1+}I_{2-} + I_{1-}I_{2+}\rangle} \\ &= \frac{2C^2S^2[\sin^2(\theta_1+\theta_2) - \cos^2(\theta_1+\theta_2)]}{2C^2S^2 + 4S^4} \\ &= \frac{(1+G)[\sin^2(\theta_1+\theta_2) - \cos^2(\theta_1+\theta_2)]}{1+3G}. \end{aligned} \tag{B1}$$

Hence, for a non-negligible gain G, the coefficient B is multiplied by $\frac{1+G}{1+3G}$, preventing any violation of the CHSH inequalities for $\frac{1+G}{1+3G} \leqslant \frac{1}{\sqrt{2}}$.

[1] C. K. Hong, Z. Y. Ou, and L. Mandel, Measurement of subpicosecond time intervals between two photons by interference, Phys. Rev. Lett. **59**, 2044 (1987).

[2] P. A. Moreau, F. Devaux, and E. Lantz, Einstein-Podolsky-Rosen paradox in twin images, Phys. Rev. Lett. **113**, 160401 (2014).

[3] M. P. Edgar, D. S. Tasca, F. Izdebski, R. E. Warburton, J. Leach, M. Agnew, G. S. Buller, R. W. Boyd, and M. J. Padgett, Imaging high-dimensional spatial entanglement with a camera, Nat. Commun. **3**, 984 (2012).

[4] A. Aspect, J. Dalibard, and G. Roger, Experimental test of Bell's inequalities using time-varying analyzers, Phys. Rev. Lett. **49**, 1804 (1982).

[5] J. Beugnon, M. P. A. Jones, J. Dingjan, B. Darquié, G. Messin, A. Browaeys, and P. Grangier, Quantum interference between two single photons emitted by independently trapped atoms, Nature (London) **440**, 779 (2006).

[6] N. Somaschi *et al.*, Near-optimal single-photon sources in the solid state, Nat. Photonics **10**, 340 (2016).

[7] B. Courme, C. Vernière, P. Svihra, S. Gigan, A. Nomerotski, and H. Defienne, Quantifying high-dimensional spatial entanglement with a single-photon-sensitive time-stamping camera, Opt. Lett. **48**, 3439 (2023).

[8] G. Weihs, T. Jennewein, C. Simon, H. Weinfurter, and A. Zeilinger, Violation of Bell's inequality under strict einstein locality conditions, Phys. Rev. Lett. **81**, 5039 (1998).

[9] M. Giustina *et al.*, Significant-loophole-free test of Bell's theorem with entangled photons, Phys. Rev. Lett. **115**, 250401 (2015).

[10] L. K. Shalm *et al.*, Strong loophole-free test of local realism, Phys. Rev. Lett. **115**, 250402 (2015).

[11] B. Hensen *et al.*, Loophole-free Bell inequality violation using electron spins separated by 1.3 kilometres, Nature (London) **526**, 682 (2015).

[12] A. J. Miller, S. W. Nam, J. M. Martinis, and A. V. Sergienko, Demonstration of a low-noise near-infrared photon counter with multiphoton discrimination, Appl. Phys. Lett. **83**, 791 (2003).

[13] W. Guo, X. Liu, Y. Wang, Q. Wei, L. F. Wei, J. Hubmayr, J. Fowler, J. Ullom, L. Vale, M. R. Vissers, and J. Gao, Counting near infrared photons with microwave kinetic inductance detectors, Appl. Phys. Lett. **110**, 212601 (2017).

[14] R. Cheng, Y. Zhou, S. Wang, M. Shen, T. Taher, and H. X. Tang, A 100-pixel photon-number-resolving detector unveiling photon statistics, Nat. Photonics **17**, 112 (2023).

[15] J. W. Pan, Z.-B. Chen, C.-Y. Lu, H. Weinfurter, A. Zeilinger, and M. Zukowski, Multiphoton entanglement and interferometry, Rev. Mod. Phys. **84**, 777 (2012).

[16] C. Fabre, Véracité et fausseté en physique. Quelle est la vraie nature de la lumière? *Journées Scientifiques annuelles de l'Institut Universitaire de France*, Toulouse, April 2–4, 2013.

[17] M. J. Werner, M. G. Raymer, M. Beck, and P. D. Drummond, Ultrashort pulsed squeezing by optical parametric amplification, Phys. Rev. A **52**, 4202 (1995).

[18] M. J. Werner and P. D. Drummond, Pulsed quadrature-phase squeezing of solitary waves in $\xi^{(2)}$ parametric waveguides, Phys. Rev. A **56**, 1508 (1997).

[19] E. Brambilla, A. Gatti, M. Bache, and L. A. Lugiato, Simultaneous near-field and far-field spatial quantum correlations in the high-gain regime of parametric down-conversion, Phys. Rev. A **69**, 023802 (2004).

[20] F. Devaux, A. Mosset, and E. Lantz, Stochastic numerical simulations of a fully spatio-temporal Hong-Ou-Mandel dip, Phys. Rev. A **100**, 013845 (2019).

[21] F. Devaux, A. Mosset, P.-A. Moreau, and E. Lantz, Imaging spatiotemporal Hong-Ou-Mandel interference of biphoton states of extremely high Schmidt number, Phys. Rev. X **10**, 031031 (2020).

[22] K. E. Cahill and R. J. Glauber, Density operators and quasiprobability distributions, Phys. Rev. **177**, 1882 (1969).

[23] S. Reynaud, A. Heidmann, E. Giacobino, and C. Fabre, Quantum fluctuations in optical systems, Prog. Opt. **30**, 1 (1992).

[24] L. Mandel and E. Wolf, *Optical Coherence and Quantum Optics* (Cambridge University Press, Cambridge, 1995).

[25] L. Isserlis, On a formula for the product-moment coefficient of any order of a normal frequency distribution in any number of variables, Biometrika **12**, 134 (1918).

[26] S. Trajtenberg-Mills, A. Karnieli, N. Voloch-Bloch, E. Megidish, H. S. Eisenberg, and A. Arie, Simulating correlations of structured spontaneously down-converted photon pairs, Laser Photonics Rev. **14**, 1900321 (2020).

[27] E. Lantz, M. Mabed, and F. Devaux, Violation of Bell inequalities by stochastic simulations of Gaussian states based on their positive Wigner representation, Phys. Scr. **96**, 045103 (2021).

[28] P. G. Kwiat, K. Mattle, H. Weinfurter, A. Zeilinger, A. V. Sergienko, and Y. Shih, New high-intensity source of polarization-entangled photon pairs, Phys. Rev. Lett. **75**, 4337 (1995).

[29] J. F. Clauser, M. A. Horne, A. Shimony, and R. A. Holt, Proposed experiment to test local hidden-variable theories, Phys. Rev. Lett. **23**, 880 (1969).

[30] D. F. Walls and G. J. Milburn, *Quantum Optics*, 2nd ed. (Springer, Berlin, 2008).

[31] M. D. Reid and D. F. Walls, Violations of classical inequalities in quantum optics, Phys. Rev. A **34**, 1260 (1986).

[32] R. A. Brewster, G. Baumgartner, and Y. K. Chembo, Quantum analysis of polarization entanglement degradation induced by multiple-photon-pair generation, Phys. Rev. A **104**, 022411 (2021).

[33] A. Christ, K. Lai, A. Eckstein, K. N. Cassemiro, and C. Silberhorn, Probing multimode squeezing with correlation functions, New J. Phys. **13**, 033027 (2011).

[34] S. Massar, F. Devaux, and E. Lantz, Multiphoton correlations between quantum images, Phys. Rev. A **108**, 013705 (2023).

[35] N. Treps and C. Fabre, Criteria of quantum correlation in the measurement of continuous variables in optics, Laser Phys. **25**, 187 (2005).

[36] I. N. Agafonov, M. V. Chekhova, and G. Leuchs, Two-color bright squeezed vacuum, Phys. Rev. A **82**, 011801(R) (2010).

[37] O. Jedrkiewicz,Y.-K. Jiang, E. Brambilla, A. Gatti, M. Bache, L. A. Lugiato, and P. Di Trapani, Detection of sub-shot-noise spatial correlation in high-gain parametric down conversion, Phys. Rev. Lett. **93**, 243601 (2004).

[38] J. L. Blanchet, F. Devaux, L. Furfaro, and E. Lantz, Measurement of sub-shot-noise correlations of spatial fluctuations in the photon-counting regime, Phys. Rev. Lett. **101**, 233604 (2008).

[39] G. Brida, L. Caspani, A. Gatti, M. Genovese, A. Meda, and I. R. Berchera, Measurement of sub-shot-noise spatial correlations without subtraction of background, Phys. Rev. Lett. **102**, 213602 (2009).

[40] Z. Y. Ou, E. C. Gage, B. E. Magill, and L. Mandel, Fourth-order interference technique for determining the coherence length of a light beam, J. Opt. Soc. Am. B **6**, 100 (1989).

[41] Y. S. Kim, O. Slattery, P. S. Kuo, and X. Tang, Conditions for two-photon interference with coherent pulses, Phys. Rev. A **87**, 063843 (2013).

[42] G. Soro, E. Lantz, A. Mosset, and F. Devaux, Quantum spatial correlations imaging through thick scattering media: Experiments and comparison with simulations of the biphoton wave function, J. Opt. **23**, 025201 (2021).

[43] A. Yariv, *Quantum Electronics*, 3rd ed. (Wiley, New York, 1989).

[44] J. L. Blanchet, F. Devaux, L. Furfaro, and E. Lantz, Purely spatial coincidences of twin photons in parametric spontaneous down conversion, Phys. Rev. A **81**, 043825 (2010).

[45] H. S. Eisenberg, G. Khoury, G. A. Durkin, C. Simon, and D. Bouwmeester, Quantum entanglement of a large number of photons, Phys. Rev. Lett. **93**, 193901 (2004).

[46] G. Harder, T. J. Bartley, A. E. Lita, S. W. Nam, T. Gerrits, and C. Silberhorn, Single-mode parametric-down-conversion states with 50 photons as a source for mesoscopic quantum optics, Phys. Rev. Lett. **116**, 143601 (2016).

[47] A. Mosset, F. Devaux, G. Fanjoux, and E. Lantz, Direct experimental characterization of the Bose-Einstein distribution of spatial fluctuations of spontaneous parametric down-conversion, Eur. Phys. J. D **28**, 447 (2004).

[48] J. S. Bell, *Speakable and Unspeakable in Quantum Mechanics* (Cambridge University Press, Cambridge, 1987), p. 65.

[49] D. Bohm, A suggested interpretation of the quantum theory in terms of "hidden" variables. I, Phys. Rev. **85**, 166 (1952).

[50] A. Mari and J. Eisert, Positive Wigner functions render classical simulation of quantum computation efficient, Phys. Rev. Lett. **109**, 230503 (2012).

[51] S. Rahimi-Keshari, T. C. Ralph, and C. M. Caves, Sufficient conditions for efficient classical simulation of quantum optics, Phys. Rev. X **6**, 021039 (2016).